Research Square

Preprints are preliminary reports that have not undergone peer review.
They should not be considered conclusive, used to inform clinical practice,
or referenced by the media as validated information.

The Plastic Ceiling - Opportunities and Limitations of Microbial Carbon Recovery in Crewed Spaceflight

Joseph D. Emhof
University of Florida
Adrien Kellens
University of Florida
Rachel G. Ivester
University of Florida
Allison Y. Gao
University of Florida
Jackson Bland
University of Florida
Swati Dubey
University of Florida
Camila Hernandez-Pedraza
University of Florida
Kathleen Hallisey Rubins
University of Pittsburgh
Aaron Jacob Berliner
Weill Cornell Medicine
Nils Jonathan Helmuth Averesch
n.averesch@ufl.edu

University of Florida

Article

Keywords: Space Bioprocess Engineering, Bioregenerative Life Support, Loop Closure, Carbon Recovery, Bioreactor Sizing, Biomanufacturing, Plastics Recycling, In Situ Resource Utilization, International Space Station

Posted Date: November 10th, 2026

DOI: https://doi.org/10.21203/rs.3.rs-11156921/v1

License: This work is licensed under a Creative Commons Attribution 4.0 International License.
Read Full License

Additional Declarations: No competing interests reported.

The Plastic Ceiling - Opportunities and Limitations of Microbial Carbon Recovery in Crewed Spaceflight

Joseph D. Emhof[1], Adrien Kellens[1], Rachel G. Ivester[1], Allison Y. Gao[1], Jackson Bland[1], Swati Dubey[1], Camila Hernández-Pedraza[1], Kathleen H. Rubins[4], Aaron J. Berliner[2,3], and Nils J.H. Averesch[1,3,*]

[1]Department of Microbiology and Cell Science, IFAS, University of Florida, Gainesville, Florida, USA.

[2]Department of Radiation Oncology, Weill Cornell Medicine, New York, New York, USA.

[3]Center for the Utilization of Biological Engineering in Space (CUBES), Berkeley, California, USA.

[4]Trivedi Institute for Space and Global Biomedicine, University of Pittsburgh, Pittsburgh, Pennsylvania, USA.

[*]Corresponding Author: n.averesch@ufl.edu

ABSTRACT

The International Space Station operates on an open resource model: consumables are delivered from Earth, used once, and disposed of by atmospheric re-entry or venting. While the water cycle is substantially closed and oxygen partially so, virtually all elemental carbon in food, clothing, and packaging is lost, a paradigm incompatible with the autonomy and planetary-protection demands of deep-space operations. Microbial biotechnology has repeatedly been proclaimed a route to carbon-loop closure, yet the recovery capacity of resupply-derived waste has never been quantified. Here, we deliver an empirical carbon-accounting record covering 25 years of stable ISS operations, over which logistics resupply carried approximately 87 metric tons of carbon to low Earth orbit. An accompanying Bio-Process Sizing Framework converts user-defined operational inputs into projected carbon-recovery capacities and required reactor volumes under the physical constraints of aqueous bioprocess design, cross-checking what physics permits against what extant biology delivers. Across every scenario the framework resolves, the ceiling is set by the composition of the waste stream: packaging polymers bound what biology can recover.

Keywords: Space Bioprocess Engineering; Bioregenerative Life Support; Loop Closure; Carbon Recovery; Bioreactor Sizing; Biomanufacturing; Plastics Recycling; *In Situ* Resource Utilization; International Space Station.

Introduction

Long-duration exploration beyond low Earth orbit (LEO) transforms logistics from an operational challenge into a primary systems-engineering constraint for human spaceflight[1]. As mission duration and distance from Earth increase, logistical resupply becomes progressively more constrained by launch costs and cadence, which are determined by mass and risk.

Although the International Space Station (ISS) has demonstrated the feasibility of continuous human presence in orbit for over two decades, it operates under an inherently open-resource model in which virtually all supplies are delivered from Earth, used once, and then discarded through atmospheric re-entry or venting[2]. While this paradigm is acceptable for LEO operations with regular resupply, it is ultimately incompatible with the demands of deep-space missions, where autonomy and closed-loop resource management will be essential[3].

Since its inception, the ISS has received over 500 metric tons of logistics mass[4]. Carbon is embedded within all major cargo categories, including Environmental Control and Life Support Systems (ECLSS) hardware, Science and Outfitting payloads ($\sim 29\%$ of delivered mass), and food systems ($\sim 21\%$)[5]. Crew nutrition alone introduces substantial organic carbon; each

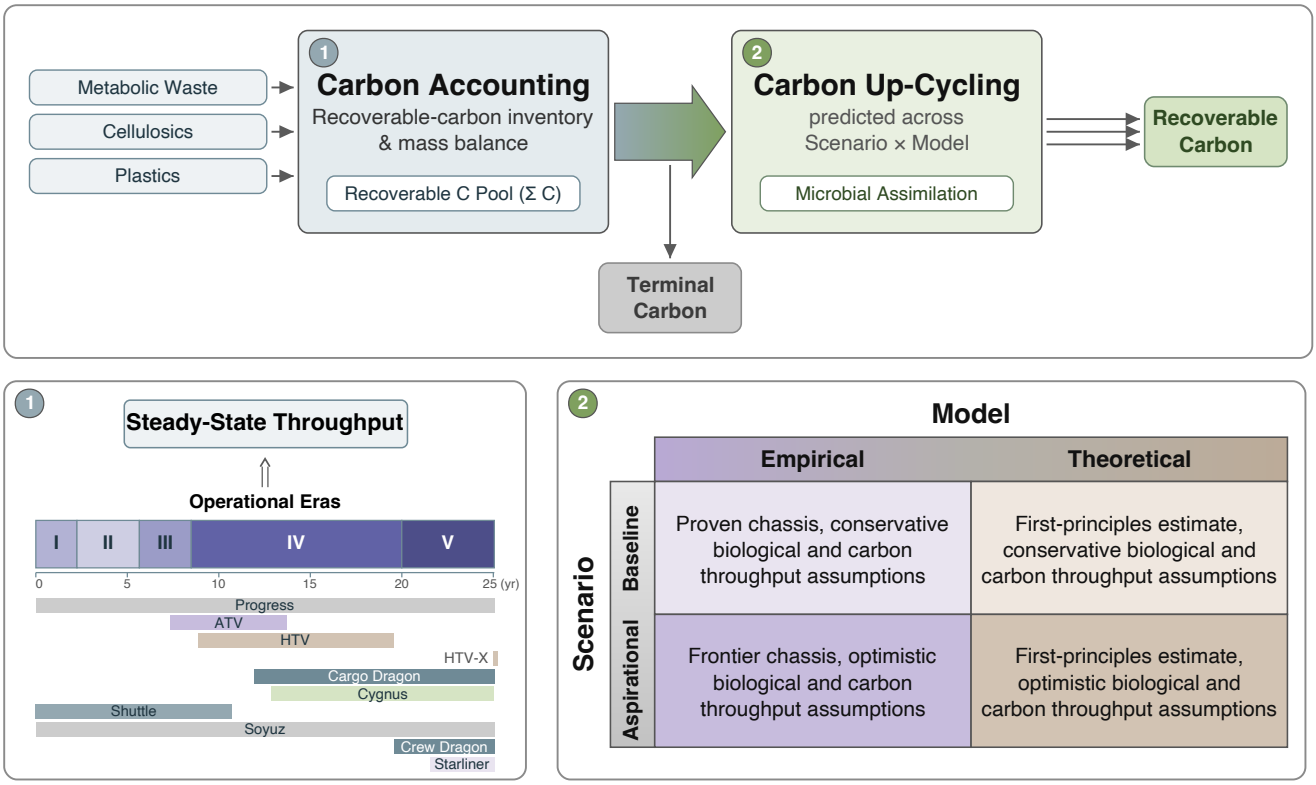


Figure 1. Overview of the analytical structure. The study proceeds in two stages, carbon accounting ① followed by carbon up-cycling ②, supported by an empirical reconstruction of the operational history and a conceptual Scenario×Model framework. **(a)** Analytical schema. Carbon-bearing waste streams enter stage ①, Carbon Accounting, which resolves the recoverable-carbon inventory and mass balance into pools of recoverable carbon (Σ C). These pools pass to stage ②, Carbon Up-Cycling, where microbial assimilation fixes the amenable carbon as a recovered fraction (biomass and co-products), while the remaining balance bypasses the bioprocesses as a terminal fraction. Matching badge colors link each stage to its supporting panel in (b) and (c). **(b)** Empirical basis for stage ①. Five era segments span the reconstructed operational history on a shared timeline; segment width is proportional to era duration, and shading encodes each era's mean crew complement, darker for larger crews. Beneath the axis, bars give the service span of each visiting cargo and crew vehicle: Progress and Soyuz share a fill (common operator), as do HTV and HTV-X (successor vehicles) and Cargo and Crew Dragon (common vehicle family), while all other fills are distinct from each other and from the era shading. The era reconstruction supplies the steady-state throughput that sets the input magnitudes in (a). **(c)** Conceptual basis for stage ②. The Scenario×Model matrix defines the four parameterizations across which up-cycling is evaluated. Columns fix the model and are distinguished by hue: Empirical, parameterized from demonstrated chassis performance, and Theoretical, derived from reaction stoichiometry, gas–liquid mass transfer, and kinetics. Rows fix the scenario and are distinguished by shade: Baseline and Aspirational, the latter carrying more optimistic biological and carbon-throughput assumptions. The scenario axis spans a conservative and an optimistic expectation, whereas the two models are independent estimates of the same quantity that cross-check rather than bound one another.

astronaut receives approximately 2.4 kg of food per day (including packaging), corresponding to $\sim$ 1 kg of carbon-rich dry matter[6]. Packaging films, polymer foams, textiles, and laboratory consumables continuously add to this influx of carbonaceous material. However, only a small fraction of these materials returns to Earth; the majority is metabolized and ultimately vented into space or loaded onto disposal vehicles and destroyed upon re-entry[7]. The ISS has achieved substantial closure of water and partial closure of oxygen cycles through advanced regenerative subsystems. The Water Recovery System (WRS) and Urine Processor Assembly (UPA) now approach recovery efficiencies near 98%[8,9]. The Sabatier system is designed to recover oxygen by converting waste carbon dioxide and hydrogen to water and methane; water is then split into hydrogen and oxygen via electrolysis[10]. Despite a theoretical reaction efficiency near 100% for modern Sabatier reactors, actual oxygen recovery efficiency on ISS is $\sim$ 50% due to limited onboard hydrogen reserves and hardware issues[10,11]. In addition, the methane produced is treated as waste and is vented along with excess carbon dioxide. Solid organic waste and synthetic polymers are similarly discarded rather than reused or recycled[12]. The carbon cycle aboard the ISS therefore remains predominantly linear.

From both engineering and economic perspectives, this is wasteful. Launch costs to LEO remain high on a per kilogram basis, and costs will increase significantly for cargo transport to the Moon or Mars. In addition, delays or failures in resupply beyond LEO could interrupt life-support-relevant deliveries. Carbon-bearing waste streams represent a valuable, untapped resource that could augment life support systems and associated functions through biomanufacturing. Waste carbon is therefore a candidate feedstock for *in situ* resource utilization (ISRU) and loop-closure, rather than a stream to be discarded.

Despite its strategic importance, a comprehensive, system-level carbon mass balance of ISS operations has yet to be established, though the necessary data largely exist. While published analyses quantify logistics mass, individual ECLSS subsystem performance, and waste production, none integrate these datasets into a unified carbon-flow inventory encompassing gaseous, liquid, and solid streams within consistent system boundaries. This lack of integration prevents rigorous identification of dominant loss pathways, accurate quantification of recoverable fractions, and effective evaluation of regenerative offsets on a mass-balance basis.

In this study, the ISS is treated as a steady-state orbital habitat that is resolved into five multi-year operational eras. Over these timescales, accumulation of carbon within the station is negligible relative to throughput, allowing carbon inputs to be balanced against outputs and transformations under steady-state assumptions. Long-term averages therefore converge to stable mean fluxes, even if individual missions and crew complements vary. This approach enables a closed carbon mass balance to be established that is internally consistent and readily transferable to other crew-centric mission architectures. A system-level carbon accounting model is constructed from technical documentation and subsystem performance data to quantify carbon inflows, internal transformations, temporary storage, and losses. Carbon streams are classified and resolved in terms of magnitude and biological accessibility. This distinction enables the separation of readily bioavailable carbon (e.g., metabolic carbon dioxide, food residues, soluble organics) from carbon embedded in structurally persistent synthetic polymers and composite materials that are difficult to recover under off-Earth operational constraints. It also establishes a quantitative basis for evaluating material selection strategies in future mission architectures where loop-closure is treated as a

boundary condition from the outset of design, not addressed after logistics chains are already fixed. Building on this inventory, a configurable Bio-Process Sizing Framework is introduced that converts available carbon fluxes into equivalent production capacities under parameterized rate and yield assumptions. The framework applies different bioconversion mechanisms based on the bioavailability of the respective waste streams, while remaining agnostic of the target product(s). This supports scenario analysis across different mission architectures and can be readily adapted to, e.g., lunar parameters in terms of durations, crew sizes, and closure by substituting mission-specific boundary conditions. Figure 1 summarizes the structure of the analysis: the carbon-accounting stage that establishes the recoverable inventory, the up-cycling stage that converts it, and the Scenario×Model design across which the up-cycling projections are reported.

Results

Carbon Accounting

The ISS steady-state carbon mass balances presented here resolve carbon throughput of logistical resupply for operational upkeep in terms of carbon mass per-crew-member, per-year. This normalization removes the confounding effect of a crew complement that varied substantially across the operational record, making the resulting inventory transferable to habitat architectures of different sizes. Across the five operational eras spanning November 2000 to November 2025, comprising 132.6 cumulative person-years at a time-weighted mean complement of 5.29, logistics resupply delivers 655.9 kg_C/(person·yr), equivalent to 3,470 kg_C/yr at the mean complement. The per-stream derivation and its full source trace are given in the Supplementary Methods.

Figure 2a traces this carbon from the consumable categories in which it is launched to the streams in which it is ultimately discarded. Packaging is the single largest source, at 282.8 kg_C/(person·yr), or 43.1% of the total, followed by food at 172.3 (26.3%), personal supplies at 127.4 (19.4%) and clothing at 73.4 (11.2%). That packaging exceeds food as a carbon source is the first indication that the ISS carbon budget is dominated not by metabolic activity but by the material overhead of delivering consumables to orbit.

On the disposal side, the same carbon resolves into six streams of markedly different biological accessibility. Respired carbon dioxide accounts for 107.5 kg_C/(person·yr) and wet organic waste, comprising food residues and human waste, for a further 64.8 kg_C/(person·yr). Cellulosic solids, comprising cotton textiles, paper products, wipes and liners, contribute 116.1 kg_C/(person·yr). The remainder is synthetic polymer: 42.6 kg_C/(person·yr) as polyesters, 15.2 kg_C/(person·yr) as polyamides, and 309.6 kg_C/(person·yr) as recalcitrant plastics, predominantly polyolefin packaging films and aramid-rich Cargo Transfer Bag (CTB) textile.

The composition of this inventory, rather than its magnitude, is what constrains recovery. Synthetic polymers together account for 367.5 kg_C/(person·yr), or 56.0% of all accounted carbon, and recalcitrant plastics alone account for 309.6, or 47.2%. By comparison, the metabolic streams that regenerative life support has historically targeted (respired CO_2 and wet organics) together represent 172.3 kg_C/(person·yr), or 26.3%, and cellulosics a further 17.7%. A majority of the carbon aboard

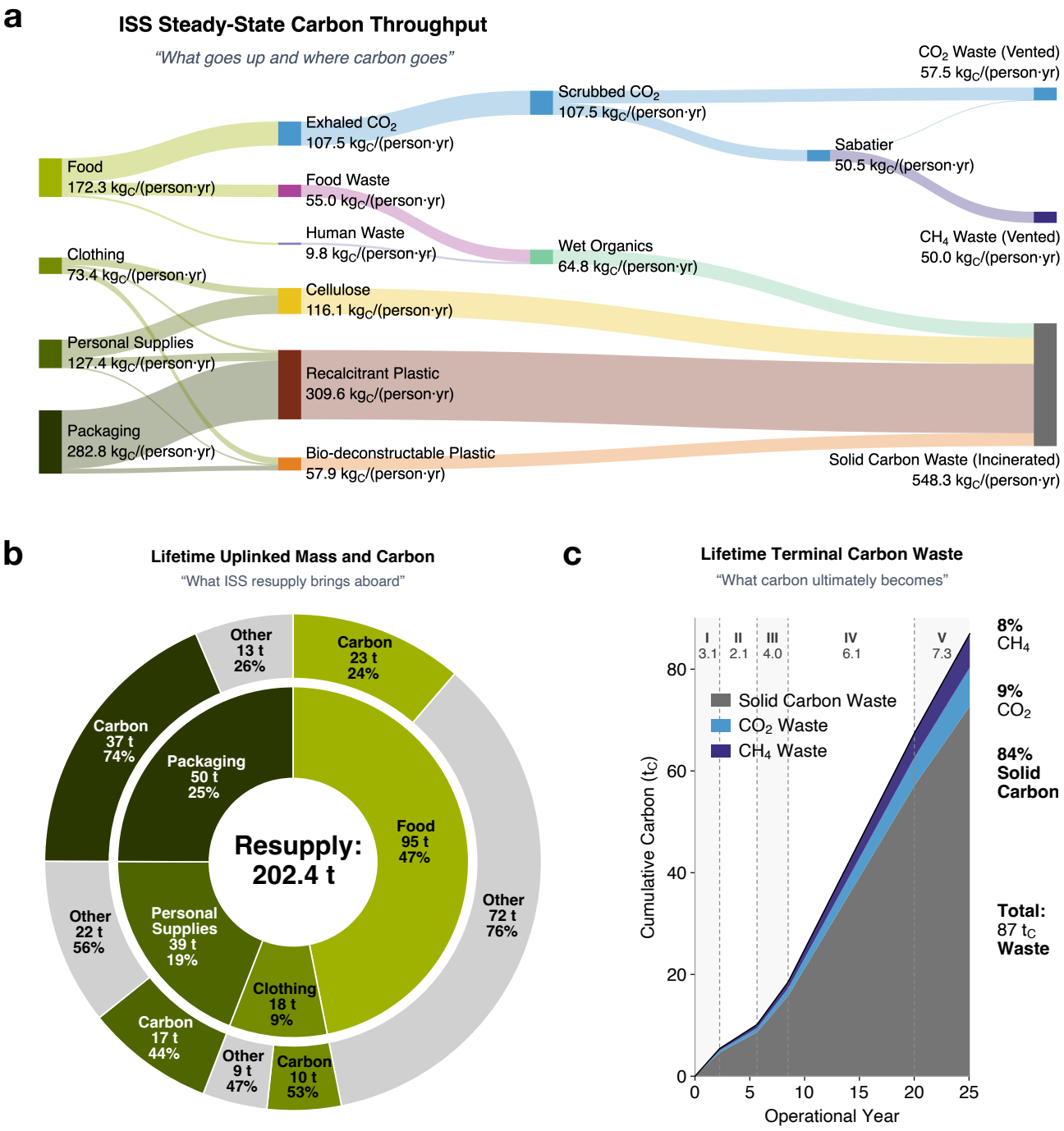


Figure 2. ISS carbon inputs and terminal fate. **(a)** Carbon flow from the four resupply classes, through the waste streams in which it is discarded, to the three terminal fates, per crew member per year. Band width is proportional to carbon flux. **(b)** Uplinked mass over the operational record by resupply class. The inner ring gives each class as a share of total uplinked mass, stated at the center; the outer ring divides each class into its carbon and non-carbon (other) mass, with percentages expressed within the class. **(c)** Cumulative terminal carbon over the operational record, stacked by fate. Shaded bands mark the five operational eras, each labeled with its mean crew complement, and the shares at right give each fate's contribution to the lifetime total. Panel (a) is on an annual per-crew-member basis and panels (b) and (c) are on a lifetime basis.

is therefore locked in the material class least amenable to biological conversion (Supplementary Figure 1).

The fate of that carbon is correspondingly linear. Of the 655.9 kg_C/(person·yr) entering the system, 548.3 (83.6%) leaves

as solid waste destined for destructive re-entry[7], and the remaining 107.5 (16.4%) is vented. The venting pathway is instructive: of the respired carbon dioxide scrubbed from cabin air, approximately 50.5 kg_C/(person·yr) is routed to the Sabatier reactor, and 57.0 is vented directly. The water produced via the Sabatier reaction is retained and electrolyzed to recover oxygen, but the co-produced 50.0 kg_C/(person·yr) in methane is vented[10], and the remaining 0.5 leaves as unreacted CO_2. The only carbon-processing step within the ISS ECLSS therefore retains no carbon; it changes only the form in which carbon is vented.

Figure 2b and Figure 2c extrapolate data from the annual mass balance across the 25-year operational lifetime of the ISS to estimate the total magnitude of this carbon flow. In order to sustain baseline operations over this time frame, 202.4 t of consumables containing 87.0 t_C were launched to ISS (Figure 2b). The carbon intensity of that mass differs systematically by resupply class: packaging and CTB textiles are near-stoichiometrically carbon-dense while food carries substantial water and mineral content. The categories that dominate uplinked mass and those that dominate uplinked carbon are therefore not the same, and mass-based logistics accounting alone does not identify where recoverable carbon resides. Aggregated over the operational record, Figure 2c shows cumulative terminal carbon reaching 87.0 t_C, of which incinerated solid waste constitutes 83.6%, vented carbon dioxide 8.8%, and vented methane 7.6%.

Carbon Up-Cycling

Two features of the inventory frame the up-cycling analysis. First, the recoverable pool is bounded by composition: a bioprocessing architecture that addresses only the metabolic streams, however efficiently, reaches at most about a quarter of the carbon aboard. Second, the streams differ by orders of magnitude in how readily their carbon can be liberated, from directly assimilable gases and soluble species, through hydrolyzable cellulosics and bio-deconstructable polymers, to recalcitrant polymers that require thermochemical deconstruction before any biological step. The Bio-Process Sizing Framework (BPSF) quantifies that second distinction.

Converting the accounted carbon into biomass requires first that it be made bioavailable, and then that a chassis capable of assimilating it be assigned. Hence, three interconversions (anaerobic digestion of wet organics, pyrolysis of recalcitrant plastics, and Sabatier methanation of the pooled carbon dioxide) redistribute the six accounted streams into eight substrate pools: carbon dioxide, carbon monoxide, methane, volatile fatty acids (VFAs), residual wet organics, cellulose, polyesters and polyamides. An allocation matrix then partitions each pool among the chassis classes able to use it (autotrophs, acetogens, methanotrophs, heterotrophs) subject to a per-pool constraint that the assigned fractions sum to no more than unity.

Projections are reported over a two-by-two design. The scenario axis, Baseline against Aspirational, varies how much of each stream is made accessible and how aggressively each process is operated. The model axis, Theoretical against Empirical, varies the provenance of the bioprocess parameters: a first-principles estimate derived from stoichiometry, gas–liquid mass transfer and kinetics, or the measured performance of specific organisms. The two axes are independent, so each of the four combinations is a self-consistent parameterization rather than a scenario in the narrative sense.

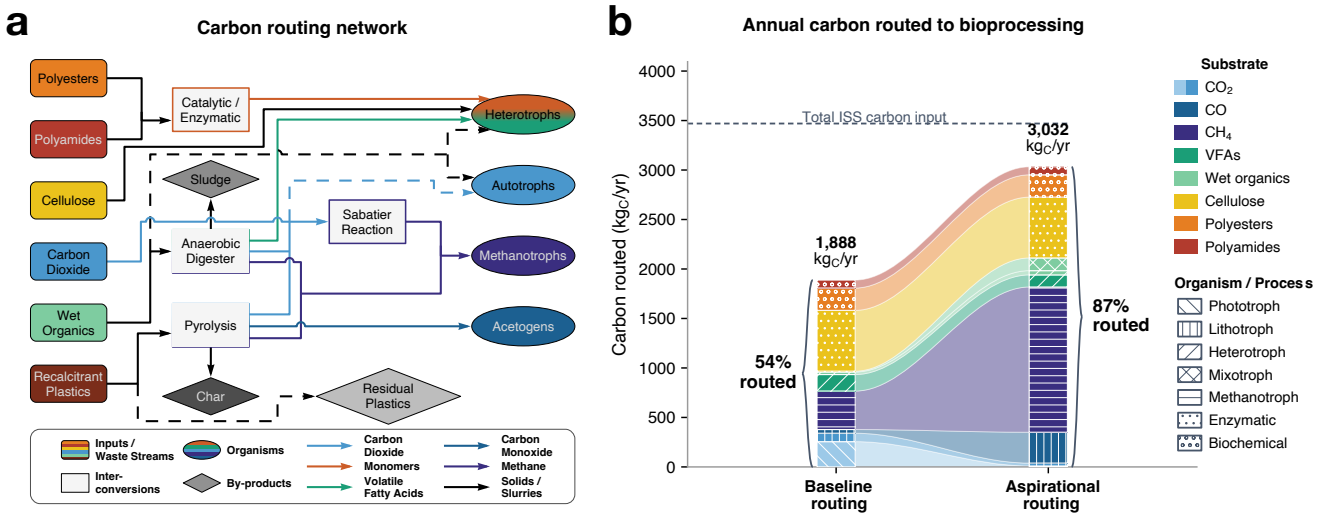


Figure 3. Carbon routing from waste streams to microbial chassis. (a) Routing network. Waste-stream inputs (colored boxes) pass through interconversions (white boxes) to the chassis classes that assimilate them (ellipses); by-products are shown as gray diamonds. Arrow color identifies the carbon species carried, and dashed arrows mark streams that bypass an interconversion. **(b)** Annual carbon routed to bioprocessing under Baseline and Aspirational routing, stacked by route. Fill color identifies the substrate and hatch pattern the organism or process class, and ribbons connect the same route across the two scenarios. The dashed line marks total ISS carbon input, and the bracket beside each bar gives the fraction routed.

Routing and Throughput

The first major sorting point in the framework is a network of interconversion steps that converts raw waste streams into substrate pools that distinct microbial chassis can use as a carbon source (Figure 3). These pools are then used as the post-processing carbon inputs for the Baseline and Aspirational configurations. Figure 3b reveals an over 60% increase from the Baseline to Aspirational scenarios, which traces almost entirely to the larger share of recalcitrant plastics routed to pyrolysis (Figure 3a). The contributions from polyamides, polyesters, and cellulose remain unchanged between scenarios, whereas that of volatile fatty acids falls by about a quarter, as half rather than nine-tenths of the wet organics are digested. In contrast, the Aspirational scenario shows markedly higher inputs of wet organics to heterotrophic and mixotrophic processing, as well as elevated carbon monoxide (CO) and methane (CH_4) fluxes. However, carbon dioxide (CO_2) inputs to photoautotrophic and lithoautotrophic pathways are reduced in the Aspirational case, because 95% rather than 50% of the pooled CO_2 is methanated in the Sabatier step.

The dominant carbon sources in the Baseline configuration are, in order: cellulose, CH_4, CO_2, and polyesters. In the Aspirational configuration, the order shifts to methane, cellulose, CO, and polyesters. The two scenarios also employ different technologies for pyrolyzing the recalcitrant plastics: the Aspirational scenario uses Microwave-Assisted Pyrolysis (MAP), which directs 14% of the pyrolyzed carbon to CO_2, against 24% for the Plasma Pyrolysis (Plas-Pyro) route used in the Baseline scenario. Because nine times as much plastic is pyrolyzed under Aspirational routing, MAP nonetheless contributes more CO_2 in absolute terms; the decline in CO_2 available to the autotrophic routes stems from the Sabatier routing, not from the pyrolysis technology. The pyrolysis routing split is the single largest scenario lever governing throughput; tuning pyrolysis temperature, residence time, and catalyst loading pre-shapes the carbon pool, either easing the metabolic burden on specialized microbes or

expanding the flexibility of a more generalist consortium.

In the Baseline scenario, the carbon pool is polymer-deconstruction-dominated, whereas the Aspirational configuration is gas-phase-dominated, reflecting a qualitative shift in pool composition (Figure 3b). The lower CO_2 share of MAP likely stems from its milder heating profile, which favors partial deoxygenation pathways and preserves more reduced carbon species that subsequently emerge as CH_4 and CO in the pyrolysis gas[13–15]. The heightened CO and CH_4 fluxes of the Aspirational case, funneled into acetogenic and methanotrophic bioprocesses, respectively, reflect this product distribution together with the ninefold larger quantity pyrolyzed; for CH_4, the Sabatier step contributes as much again, supplying half of the Aspirational methane pool.

Biomass Generation and Reactor Sizing

The conversion of the post-processing carbon throughput into biomass is evaluated under two distinct biological models. The empirical model parameterizes each route from the performance of specific organisms reported in the literature, whereas the theoretical model derives the corresponding capacities from first-principles limits on mass transfer, light delivery, and reaction kinetics. Within each model, the Baseline and Aspirational scenarios operate on the Baseline and Aspirational carbon throughput, respectively, and span a realistic and an ambitious expectation for bioprocessing with pre-existing organisms: a typical against a highly optimized chassis in the empirical model, and conservative against optimistic process parameters in the theoretical one. For example, the polyester and polyamide routes are depolymerization-limited under Baseline assumptions, whereas the Aspirational case assumes monomer is supplied and taken up directly.

The consequences of carbon routing on biomass production and infrastructure requirements are summarized in Figure 4. Routing reshapes the distribution of biomass across pathways (Figure 4a). Under the Baseline scenario, biomass production is dominated by valorization of cellulose in both models (512 and 565 kg/yr in the theoretical and empirical models, respectively), followed by methanotrophic fixation of CH_4 (351 and 541 kg/yr), and photoautotrophic fixation of CO_2 (279 and 255 kg/yr). Together, these three routes represent approximately two-thirds of the total biomass produced in the theoretical model (67%) and close to four-fifths in the empirical model (80%); no other single pathway exceeds 190 kg/yr in either model. Under the Aspirational scenario, the distribution is increasingly uneven as a substantial part of the carbon redirects to methanotrophs because more of the recalcitrant plastic is routed to pyrolysis and more of the CO_2 is methanated in the Sabatier step. Methanotroph biomass production increases from 351 to 1,514 kg/yr in the theoretical model and from 541 to 1,514 kg/yr in the empirical model, making this pathway the dominant contributor to biomass production in both cases. The pathway valorizing carbon monoxide also increases from 11 to 116 kg/yr theoretically and from 1 to 119 kg/yr empirically. Mixotrophic conversion of wet organics rises from 9 to 179 kg/yr in the theoretical model. The empirical model resolves no wet-organic routes, since no single organism has been reported that represents the mixed cultures these pathways assume. Conversely, the contribution of photoautotrophs drops drastically, from 279 to 12 kg/yr in the theoretical model and from 255 to 12 kg/yr in the empirical model, due to direct reduction of carbon throughput available in the CO_2 form, after thermochemical conversion. Cellulose remains an important contributor to biomass production under the Aspirational scenario in both theoretical and empirical models (594 and

175 756 kg/yr), although its relative contribution decreases strongly as pathways utilizing reduced carbon intermediates become

176 increasingly dominant. This redistribution toward methanotrophs drives the reactor-volume comparison in Figure 4c.

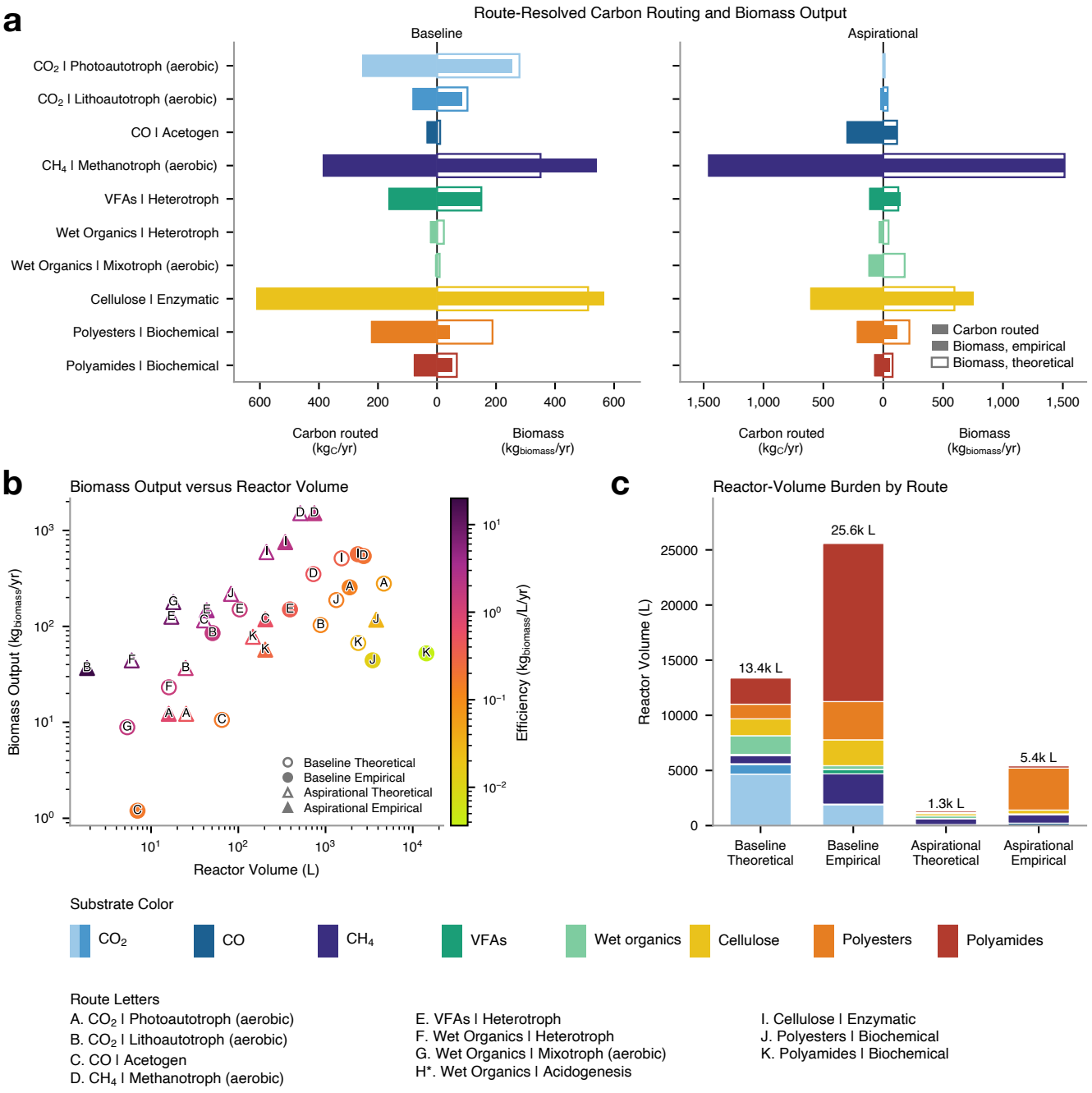


Figure 4. Route-resolved biomass output and reactor-volume burden. Letters identify routes throughout and fill color identifies the substrate in (a) and (c), both keyed beneath the figure; in (a) and (b), filled marks give the empirical estimate and open marks the theoretical. **(a)** Annual carbon routed (left of each axis) and biomass produced (right) for each route, under Baseline and Aspirational routing. **(b)** Biomass output against reactor volume for each route, on logarithmic axes. Marker shape identifies the scenario (circles Baseline, triangles Aspirational), and marker color gives volumetric efficiency, the biomass produced per liter of reactor per year. **(c)** Total reactor volume for each Scenario×Model combination, stacked by route, for annual inputs of 1,888 kg_C/yr (Baseline) and 3,032 kg_C/yr (Aspirational). The acidogenesis route (H*) is an interconversion step that occupies reactor volume but fixes no biomass, and so appears in (c) but not in (a) or (b).

177 The two models diverge only under Aspirational routing (Supplementary Figure 2). Under Baseline routing, they agree

to within a kilogram per year, at 1,694 kg/yr empirical against 1,693 kg/yr theoretical, so the first-principles estimate and the chassis-derived one corroborate each other where the routing is conservative. Under Aspirational routing, the theoretical estimate is the higher of the two, 2,919 against 2,759 kg/yr, a gap of roughly six percent. This gap reflects the absence of wet-organic routes from the empirical model and the first-principles ceiling on depolymerization-limited rates, which no reported chassis yet attains, partly offset by cellulose, for which the reported chassis exceed the theoretical estimate.

Figure 4b shows the intrinsic efficiency of each conversion pathway, expressed as the biomass production per unit of reactor volume. The efficiency spans nearly three orders of magnitude across the different conversion pathways. Under the Aspirational empirical framework, aerobic lithoautotrophic growth on CO_2 exhibits the highest volumetric productivity (20 kg biomass/L/yr, from high-cell-density autotrophic cultivation), followed by heterotrophic growth on VFAs (3.4 kg/L/yr), cellulose valorization (2.2 kg/L/yr), and methanotrophic growth (2.0 kg/L/yr). In contrast, polyester and polyamide conversion display the lowest efficiencies, at 0.03 and 0.28 kg biomass/L/yr, respectively; under Baseline routing, the empirical polyamide route falls further still, to 0.004 kg biomass/L/yr, as depolymerization rather than assimilation then sets the achievable rate. The theoretical framework reproduces the same broad separation between gaseous or soluble substrates and polymeric ones, but ranks the individual routes differently. There, mixo- and heterotrophic conversion of wet organics and VFAs are the most volumetrically efficient platforms, whereas lithoautotrophic CO_2 fixation ranks comparatively low. These differences come from chassis-specific biomass yields and volumetric productivities, as well as specific process limitations such as gas transfer, light exposure, hydrolysis, and enzymatic depolymerization. Carbon throughput alone is therefore not sufficient to evaluate the suitability of a conversion pathway; as with the size of the recoverable pool, the chemical form in which carbon becomes available determines how efficiently it can be converted into biomass.

These differences in biomass production efficiency directly translate into reactor volume requirements at the scale of the entire system (Figure 4c). The total required reactor volume decreases under the Aspirational scenario in comparison to Baseline, from 13.4 kL to 1.3 kL for theoretical assumptions and from 25.6 kL to 5.4 kL for the empirical assumptions, corresponding to a 90.1% reduction in the theoretical framework and a 78.8% reduction in the empirical framework. However, the empirical models require larger volumes than their theoretical counterparts in both scenarios, with the empirical estimate approximately 2-fold higher than the theoretical estimate under Baseline routing and 4-fold higher under Aspirational routing. This difference is mainly driven by the polyester and polyamide conversion routes. Together, under the Baseline scenario, polyester and polyamide inputs account for approximately 28% of the theoretical reactor volume and 70% of the empirical reactor volume (3,702 L and 17,809 L, respectively). Under the Aspirational scenario, they represent 17% of the theoretical reactor volume and nearly 75% of the empirical reactor volume (229 L and 4,011 L), with the corresponding route-resolved distributions given in Supplementary Figure 3. Despite the orders-of-magnitude differences in reactor volumes required to process these synthetic polymer inputs for each model and scenario pairing, the resulting annual biomass output varies only threefold, from 97 to 296 kg/yr (baseline empirical and aspirational theoretical, respectively). Therefore, the largest reactor volume penalty does not come from the total amount of carbon routed to these pathways, but from the low empirical carbon

processing capacity and biomass productivity associated with polymer depolymerization and biological assimilation.

Global Carbon Ledger and the Hard Ceiling

Figure 5a summarizes the annual carbon balance across theoretical and empirical modeling frameworks under Baseline and Aspirational routing scenarios. Total carbon throughput rises from ∼54% of total carbon input in the Baseline scenarios to ∼87% in the Aspirational scenarios reflecting a much greater proportion of the carbon stream being directed into conversion processes. All the corresponding numerical values for this figure are given in the 'Scenarios' sheet of Supplementary Data 1.

Biomass fixation efficiency ranges from 24.4% to 42.1%, and carbon recovery as CO_2e from 31.0% to 47.6%, across the four scenarios evaluated here. The empirical and theoretical Baseline cases agree closely: recoverable CO_2e of 31% (1,075 kg_C/yr) against 31% (1,076 kg_C/yr), and biomass fixation of 24% (847 kg_C/yr) for both models. Consistently, the Aspirational scenarios have better carbon recovery efficiencies than the corresponding Baseline scenarios. For example, Aspirational routing reduces the fraction of remaining plastics from 42.5% to only 4.7% (164 kg_C/yr), increasing overall conversion efficiency and carbon utilization. However, the bioprocessing pathways favored need not be the same across each of these scenarios. For instance, in the theoretical Aspirational scenario, recoverable CO_2e becomes the dominant fate, accounting for 45.3% of the total carbon input (1,573 kg_C/yr), with biomass fixation accounting for a comparable 42.1% (1,459 kg_C/yr). The empirical Aspirational scenario shifts further in the same direction, with recoverable CO_2e reaching 47.6% (1,653 kg_C/yr)

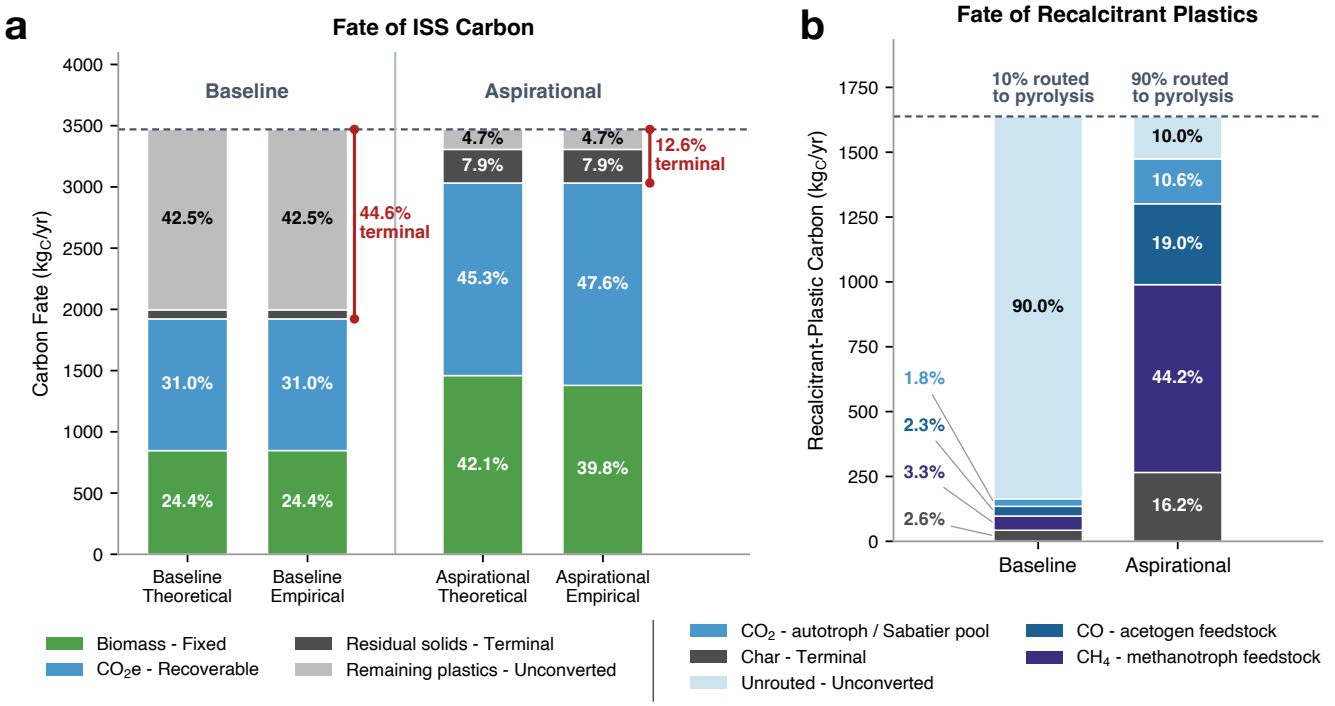


Figure 5. Fate of ISS carbon and of the recalcitrant-plastic fraction. (a) Annual ISS carbon input partitioned by fate for each Scenario×Model combination: biomass, recoverable CO_2-equivalent carbon, residual solids, and plastics remaining unconverted. The dashed line marks total carbon input, and the red bracket spans the terminal fraction, comprising residual solids and remaining plastics. **(b)** The recalcitrant-plastic input partitioned by product under Baseline and Aspirational routing, which send 10% and 90% of it to pyrolysis, respectively. Segments give the pyrolysis products, CH_4, CO, and CO_2 as bioprocess feedstocks and char as a terminal residue, together with the unrouted remainder, which is the remaining-plastics pool of (a). The dashed line marks the recalcitrant-plastic input. Pyrolysis yields do not depend on the bioprocess model, so (b) shows one bar per scenario.

while biomass fixation falls to 39.8% (1,379 kg_C/yr). Residual solids, including anaerobic digestion sludge and pyrolysis char, represent a relatively small but consistent terminal sink across all scenarios, increasing from about 2.1% in Baseline routing to 7.9% in Aspirational routing due to the larger fraction of material processed. When combined with unconverted plastics, the total terminal/lost carbon pool declines from 44.6% in Baseline scenarios to 12.6% in Aspirational scenarios, a reduction of more than threefold, achieved through microbial biomass formation and gaseous carbon streams.

Figure 5b illustrates the fate of recalcitrant plastic-derived carbon under Baseline and Aspirational pyrolysis routing strategies for an annual input stream of 1,638 kg_C/yr; the underlying values are given in Supplementary Data 1. The two scenarios differ substantially in the proportion of material directed toward conversion pathways versus remaining unprocessed. Under the Baseline scenario, only 10% of the recalcitrant plastics are routed to pyrolysis, resulting in 90% of the carbon remaining unrouted and therefore effectively unconverted. Only small fractions of carbon are transformed into useful gaseous intermediates, including CH_4 (3.3%), CO (2.3%), and CO_2 (1.8%), while char formation accounts for 2.6% of the total carbon stream. In contrast, the Aspirational routing strategy directs 90% of the recalcitrant plastics toward pyrolysis, improving carbon recovery and conversion efficiency. Methane is the dominant product pool (44.2%), followed by carbon monoxide (19.0%) and carbon dioxide (10.6%), while terminal char accounts for 16.2%. Consequently, the fraction of unrouted plastics decreases from 90% to 10%, and 12.6% of total carbon input remains terminal even under Aspirational routing.

Discussion

This study quantifies, for the first time, the scale of carbon loss under the ISS's current carbon-management strategy. Organic carbon introduced through food, crew metabolism, packaging, and other consumables is ultimately lost through venting or disposal rather than being recycled into productive use[7]. The carbon-accounting model developed here, built on a quasi-steady-state treatment of ISS operations, indicates that a substantial fraction of this carbon could instead support regenerative carbon-utilization strategies.

The two allocation matrices share a single structure and differ only in how the CO_2 and wet-organic pools are split between competing chassis, so the contrast between the scenarios arises chiefly upstream, in the interconversion steps. The Aspirational scenario allocates a larger fraction of reduced carbon (CH_4, CO) to methanotrophic and acetogenic chassis, whereas the Baseline scenario directs more oxidized carbon (CO_2) toward aerobic photo- and lithoautotrophs (Figure 3b). The decline in CO_2 is a downstream consequence of the Sabatier routing, which methanates 95% of the pooled CO_2 in the Aspirational configuration against 50% in the Baseline; with less inorganic carbon available, autotrophic pathways receive a smaller substrate flux. This shift has two practical implications. First, it may lower the carbon-fixation demand on autotrophic cultures, potentially simplifying reactor design or reducing nutrient inputs. Second, it places nearly half of all routed carbon on methanotrophs, on whose capacity the Aspirational configuration therefore depends; the same methane could instead be captured as a fuel stream.

A major outcome of this study is the BPSF, which provides a substrate-independent method for evaluating heterogeneous waste streams within a unified accounting structure. This enables more consistent estimation of carbon routing, recovery

efficiencies, and potential production capacities across different biomanufacturing pathways. Its two parameterizations, one derived from first principles and one from reported chassis performance, cross-check each other: they agree closely where routing is conservative and separate under Aspirational routing, where wet-organic and depolymerization-limited routes carry more of the carbon, which localizes where reactor engineering or strain improvement would most improve feasibility.

Recycling versus resupply is a long-running disagreement in space architecture. Some argue that reduced launch costs make resupply more economical than the development of complex recycling systems for LEO[16,17]. Yet the cost NASA has actually paid per kilogram of payload, as distinct from advertised launch prices, rose by about 2.8% per year in real terms between 1996 and 2024 for its uncrewed missions, with no change in trend after new providers entered the market[18]. From a sustainability and supportability perspective, an upfront investment into recycling systems becomes not only economical but imperative as mission duration and destination scale up. This is especially true given the high cost and risk of resupply failures. The BPSF offers a way to recover some of these losses by using bioavailable carbon, turning waste streams into a production input rather than a disposal problem.

While this study focuses on the ISS, the framework can also be adapted to future deep-space missions, including Lunar and Martian habitats, where logistical resupply will be far more constrained. Long-duration exploration missions will require increasingly autonomous, self-sustaining life-support systems, for which carbon recovery is essential[19–24]. Treating carbon loop-closure as integral to mission architecture–rather than something addressed once packaging material choices are already locked in–is the shift this framework supports. The carbon fluxes quantified here are turned into a basis for sizing production capacity, and regenerative offsets are evaluated on a mass-balance basis. As mission planning shifts toward *in situ* resource utilization and sustained extraterrestrial presence, space biomanufacturing needs to be built into mission architecture from the outset rather than added after the fact[25–29].

The Theoretical and Empirical models are not nested, and neither is intended as a bound on the other. They are two independent estimates of the same quantity, derived from different premises, and their agreement is therefore a check on both. Where they converge, the underlying assumptions are mutually corroborated, and where they diverge, the divergence localizes the assumption at fault.

Together, these results indicate that carbon routing and biological performance are two complementary levers in the design of a biomanufacturing system. Routing determines the chemical form and the quantity of carbon that could be directed to bioprocesses, whereas the performance of different microbial chassis determines the biomass production amount as well as the associated infrastructure requirements. Starting from the carbon accounting, the BPSF routes carbon streams to biomass production and reactor sizing; rather than evaluating recycling strategies solely according to the quantity of carbon recovered, it allows them to be compared according to the biomass they can generate and the infrastructure required to achieve it. This is why routing and biological performance must be optimized jointly, rather than treated as separable levers. The BPSF thereby provides a quantitative framework for selecting combinations of thermochemical and biological conversion pathways that are most compatible with the constraints of regenerative life support systems for long-duration space missions. In turn,

biomass that is not itself the target of a biomanufacturing process could be routed to alternative bioprocesses to produce food[30], pharmaceuticals[31], vitamins[32], oils[33], fuels[34], biopolymers[35], and other mission-critical products.

As established above, packaging-derived polymers dominate the carbon budget, polyolefins and aramid together account for over three-quarters of its recalcitrant fraction, and the metabolic streams regenerative life support has historically targeted make up barely a quarter of it. The recoverable pool is bounded by this waste stream composition rather than by biology. Even under the most favorable routing considered here, 12.6% of carbon remains terminal, and that residue is plastic-derived, as pyrolysis char or as the fraction not routed to pyrolysis. Across the operational record, the polymer stream as a whole amounts to 78 t, 39% of the uplinked consumables mass, carried to orbit and then destroyed on re-entry: a mass of polymer feedstock equivalent to roughly 55 BEAM-class modules, or on an areal-mass basis some 880 m^3 of expandable pressurized volume, against the ~390 m^3 of habitable volume the ISS actually provides. The comparison is one of polymer mass rather than of module construction, since the mass of an expandable module is predominantly restraint layer, shielding, and metal structure.

Volume constrains how recovery is engineered rather than how much carbon can be recovered. The required culture volume amounts to 3.4–6.6% of ISS habitable volume under Baseline routing and to under 1.5% under Aspirational routing. These are working volumes, exclusive of reactor hardware, utilities, and headspace, so the installed footprint would be larger still: a substantive allocation under Baseline routing, but unlikely to be the binding constraint under Aspirational routing. Beyond LEO, the open-loop paradigm becomes a non-viable option, as opposed to merely wasteful. Destructive re-entry does not exist as a disposal route on the surface of the Moon or Mars, venting is constrained by planetary-protection requirements, and resupply cadence lengthens from months to years. The quantities involved are not marginal: under the ISS-derived logistics assumptions used here, a lunar surface crew of four sustained for one year would accumulate 2.6 t_C, 1.5 t_C of it in polymer alone. A four-crewmember expedition to Mars over 1,000 days would accumulate 7.2 t_C, 4.0 t_C of it in polymer, none of which can be easily discarded, while at the same time resupply is likely unable to keep pace with the amount of carbon leaving the system.

The reconstruction transfers to those architectures because logistics composition is largely inherited. ISS-era manifests derive substantially from Space Shuttle-era packaging and soft-goods standards, making the stream composition reconstructed here a reasonable prior for near-term lunar logistics, and the framework is parameterized to be re-run against revised manifests as they emerge. That inheritance is not binding on the commercial LEO destinations now under development, whose logistics chains are still being defined and whose manifests a single operator can specify in a way that a multi-agency partnership never could. The most consequential intervention this analysis identifies therefore lies upstream of any bioprocess, specifying primary packaging and soft goods in biologically tractable polymers. Polyesters and aliphatic polyamides are routable within the present framework; polyolefins are not. This is a specification decision rather than a technology gap, and a transition to materials amenable to bioprocessing is the simple and inexpensive intervention. Material substitution is a one-time change carrying no recurring mass, power, thermal, or crew-time penalty, whereas bioprocessing infrastructure to recover recalcitrant plastics carries recurring mass, power, thermal, and crew-time costs for as long as it operates. Thus, a choice made before

a supply chain is established would be far cheaper than retrofitting a loop into a stream never intended to support one. On the other hand, it is difficult to match the material properties of the current recalcitrant polymers used in the ISS logistical pipeline in terms of biological and chemical inertness, and, most importantly, non-flammability. Beyond spaceflight, the same mass-transfer-constrained sizing applies to terrestrial CO_2-, CO-, CH_4- and waste-derived bioproduction, where the constraint on circularity is likewise often the composition of the waste stream rather than the capability of the organism.

Methods

Reconstruction of ISS Carbon Throughput

Carbon throughput associated with logistical resupply of the International Space Station (ISS) to support continuous human occupation was reconstructed by integrating crew-time normalization, logistics mass reconstruction, material composition analysis, and metabolic mass balance modeling. The operational history of the ISS from November 2000 through November 2025 was divided into five eras defined by stable base crew complements (see SI for explicit differentiation). For each era, the total duration in days and the mean onboard population were determined from expedition schedules. Temporary increases during vehicle handovers were incorporated by estimating average overlap duration and rotation frequency. Crew-time was calculated as the product of mean crew size and era duration. A time-weighted lifetime mean crew complement was derived and used to normalize all material flows to per-person-per-year values.

Total pressurized logistics mass delivered to the ISS was reconstructed from vehicle-specific mission records. For each cargo vehicle class (Progress, Shuttle, ATV, HTV/HTV-X, Cygnus, and Cargo Dragon), the number of flights per era was compiled and multiplied by the representative logistics payload delivered per flight. For vehicles that delivered both propellant and dry cargo, propellant mass was removed to isolate pressurized logistics mass. Shuttle flights were restricted to missions carrying ISS logistics-relevant payload. Era totals were summed to obtain cumulative logistics-only upmass, which was subsequently normalized by crew-time to determine crew-normalized throughput. Carbon-containing delivered logistics mass was partitioned into one of four input categories: food, clothing, personal supplies, or packaging. Carbon-containing inputs were then separated into waste streams by carbon type: metabolic outputs (respired CO_2), wet organic waste streams (residual food, feces, urine, human detritus), cellulose-dominant solids (cotton garments, paper products, wipes, liners), and synthetic polymers (food packaging plastics, hygiene plastics, clothing polymers, and logistics textiles). Partitioning was performed such that no mass was assigned to more than one category. Cotton-based textiles were allocated exclusively to cellulose, and CTB textiles and foam packaging were treated separately from clothing and hygiene materials. Synthetic polymers were further classed by whether the backbone carries a hydrolyzable linkage for which enzymatic depolymerization has been demonstrated: polyesters and aliphatic polyamides as bio-deconstructable, and all others, including polyolefins, fluoropolymers, and aromatic polyamides (aramids), as recalcitrant.

Material masses were converted to elemental carbon mass using stoichiometric carbon mass fractions derived from representative molecular formulas. Polymer carbon fractions were calculated from monomer molecular weights. Cellulose was

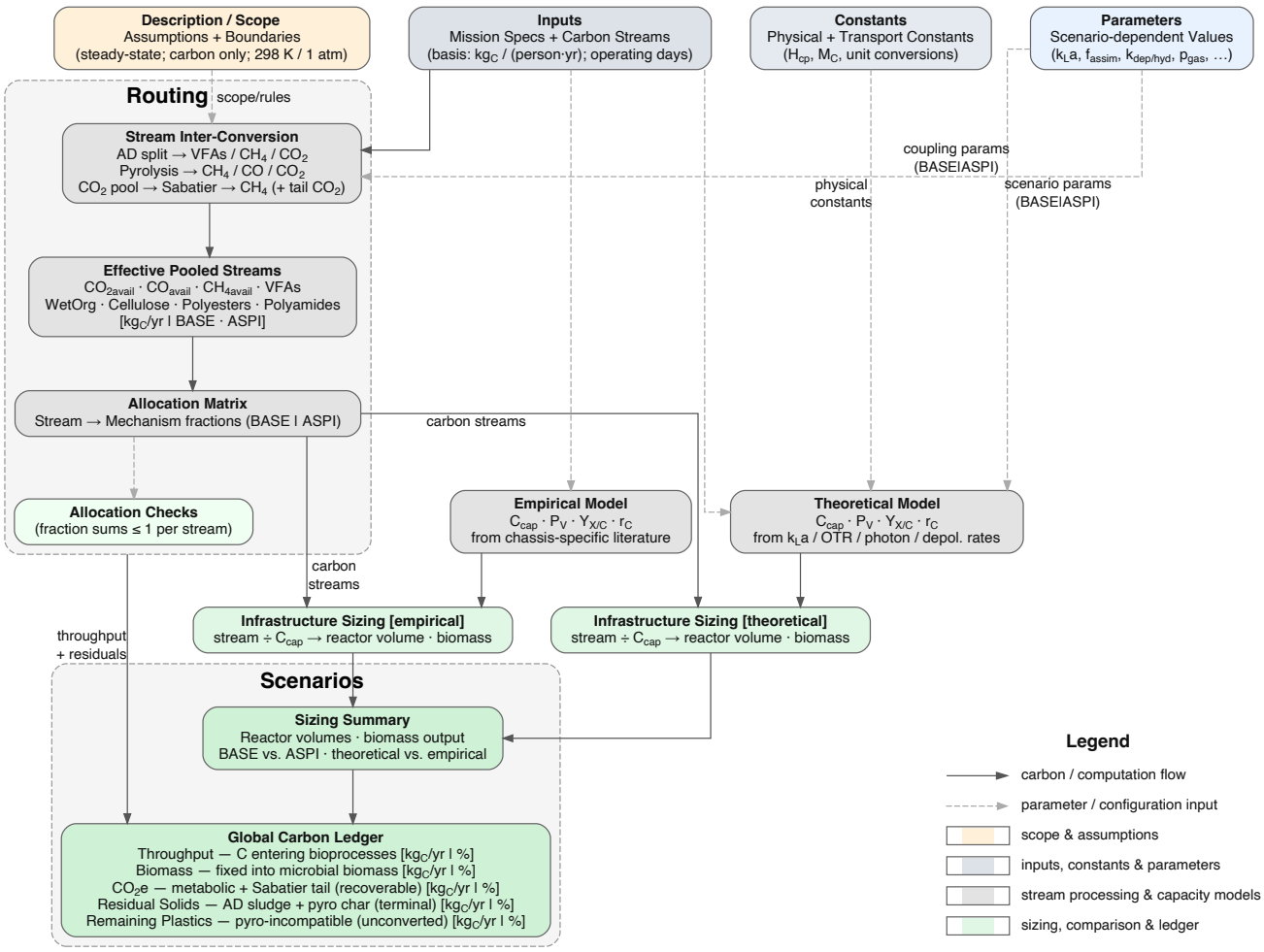


Figure 6. Architecture of the Bio-Process Sizing Framework. Flowchart of the spreadsheet workflow that converts mission carbon streams into bioprocess-sizing outputs, resolved by routing scenario and model. Configuration enters as three input groups: boundary assumptions, mission specifications with per-crew carbon-stream inventories, and the physical constants and scenario-dependent parameters that govern the downstream steps. Stream interconversion then yields effective pooled streams, resolved separately for the Baseline and Aspirational routing scenarios. An allocation matrix partitions each pooled stream among conversion mechanisms through scenario-specific fractions, subject to per-stream checks that the fractions sum to ≤ 1. Two parallel capacity models then size the infrastructure: the Empirical model takes volumetric productivity P_{V} and biomass-on-carbon yield $Y_{\mathrm{X/C}}$ from chassis-specific literature and derives the carbon uptake rate r_{C} and carbon capacity C_{cap} from them, whereas the Theoretical model derives r_{C} from mass-transfer and kinetic constraints. In each branch, stream throughput divided by carbon capacity gives reactor volume, and throughput multiplied by yield gives biomass output (Eq. (1)). A sizing summary compares reactor volume and biomass across the full Baseline/Aspirational×Empirical/Theoretical design. The global carbon ledger closes the balance, reporting throughput, biomass, recoverable CO_2e, terminal residual solids, and remaining unconverted (recalcitrant) plastics, each as both an absolute annual carbon flux and a percentage. Solid arrows trace carbon and computation flow, and dashed connectors supply parameter and configuration inputs. Node shading demarcates the four stages (scope and assumptions; inputs, constants, and parameters; stream processing and capacity models; sizing, comparison, and ledger).

assigned a carbon mass fraction of 0.44. Carbon dioxide was converted to elemental carbon using the stoichiometric mass fraction of carbon in CO_2 (12/44). For wet organic streams, carbon fractions were derived from reported moisture content and compositional data in NASA's Baseline Values and Assumptions Document (BVAD), using dietary macronutrient stoichiometry to determine dry matter carbon content.

Using these derived input categories and waste streams, a representative model of logistics-derived carbon flow through

the ISS was created. The model assumed steady-state operations aboard ISS in support of a single crew member of average mass (82 kg)[36]. Logistical input mass and waste stream values were then refined by category. For the clothing and personal supply inputs, cargo manifests and material compositions were derived from literature values[4,5,37]. For the food input category and resulting waste streams, the current ISS daily food supply planning value and representative metabolic outputs were mass balanced. For the packaging stream, soft goods logistics packaging was converted to CTB-equivalent (CTBE) values, and combined with refined packaging values from other categories, e.g., food packaging. All carbon quantities were first calculated on a per-person-per-year basis and subsequently aggregated across crew-time to obtain cumulative lifetime carbon throughput.

Formulation of the Bio-Process Sizing Framework

Figure 6 shows the architecture of the framework, from the mission inputs, physical constants, and scenario parameters, through stream interconversion and mechanism allocation, to the parallel Empirical and Theoretical capacity models and the closing global carbon ledger.

The six accounted streams were first converted into bioavailable substrate pools by three interconversions (anaerobic digestion of wet organics, pyrolysis of recalcitrant plastics, and Sabatier methanation of pooled carbon dioxide). A scenario-specific allocation matrix then divided each pool among the mechanisms able to accept it, with the fractions for any one pool summing to no more than unity. Each conversion route was characterized by its volumetric carbon processing rate r_{C} and its biomass yield on carbon $Y_{\mathrm{X/C}}$, from which the volumetric capacity, reactor volume, and annual biomass output follow as

$$C_{\mathrm{cap}} = r_{\mathrm{C}} \frac{t_{\mathrm{a}}}{1000}, \qquad V = \frac{C_{\mathrm{stream}}}{C_{\mathrm{cap}}}, \qquad X = C_{\mathrm{stream}}\, Y_{\mathrm{X/C}}, \tag{1}$$

where C_{stream} is the carbon allocated to the route per year, t_{a} the number of days per year, and the factor of 1000 converts grams to kilograms. The two capacity models differ only in how r_{C} and $Y_{\mathrm{X/C}}$ in Eq. (1) were obtained. In the Theoretical model, r_{C} was set by the physical process limiting each route: light delivery for photoautotrophy, gas–liquid mass transfer for lithoautotrophy, acetogenesis, and methanotrophy, oxygen transfer for aerobic heterotrophy, and first-order hydrolysis or depolymerization kinetics for cellulose and the synthetic polymers. In the Empirical model, both quantities were taken from the reported performance of specific organisms.

For the empirical parameterization, unified calculations were applied to all organisms to enable cross-system comparison of biomass formation efficiency. Volumetric biomass productivity (P_{V}) was defined as the amount of biomass produced per unit culture volume per day (g/L/day). The highest biomass productivity at any point was considered and then normalized to a 24-h period. Biomass yield on carbon ($Y_{\mathrm{X/C}}$) was calculated as the ratio of grams of dry biomass produced to grams of carbon supplied in the growth medium ($\mathrm{g_{biomass}/g_C}$), giving $r_{\mathrm{C}} = P_{\mathrm{V}}/Y_{\mathrm{X/C}}$. Based on the volumetric productivity and the biomass yield per unit of carbon, a high-performance candidate and a conventional, well-characterized reference organism were selected for each chassis class, corresponding to the Aspirational and Baseline parameterizations of the empirical model, respectively.

Three rate and yield corrections applied to the Theoretical layer, and not to the Empirical layer, whose measured parameters

embedded them implicitly. Henry's law solubilities were van 't Hoff-corrected from the tabulated 298.15 K reference to the operating temperature, whose default was 303.15 K. Growth carried a Pirt-type maintenance penalty, which lowered the observed assimilation fraction at low growth rate. A high-solids penalty reduced solid-substrate rates above a total-solids threshold. Definitions, parameter values, and the per-route derivation of r_{C} are given in the Supplementary Methods.

Data Availability

The authors confirm that the data supporting the findings of this study are available within the article and its supplementary information. The extent of the data provided is sufficient for replication of the study. Any other data that may be pertinent are available on request from the corresponding author.

Code Availability

All code used for aggregation and evaluation of the data as well as generation of the figures is available on GitHub at: https://github.com/aaronreichmenberliner/plastic-ceiling.

Acknowledgments

This study depended on cargo and logistics information that is not available in the open literature, and we are indebted to the people who made it accessible. At Leidos, we thank Christopher Gefrides (Cargo Mission Contract, Exploration Logistics Integrated Strategy Evaluation) for providing ISS packing-foam usage records and material specifications, and Alonso Fuentes, Kristie Brandon, Jaime Valverde, and Daniel E. Garcia for their generosity in discussing resupply logistics and cargo packaging practice with us. We are especially grateful to Deborah Wells for recognizing the value of the connection and initiating it.

At NASA Kennedy Space Center Deep Space Logistics, we thank Alexander D. Garcia and Jeffrey D. Smith for their sustained guidance and support of this work, and Amirah M. Mathin for introducing us to the MIDAS cargo-planning data system and for pursuing inventory and stowage records on our behalf. We further thank Randall D. Gordon for helpful discussion. At Aegis Aerospace, we thank Jonathan S. Pitt for programmatic support throughout.

Part of this work was supported by the National Aeronautics and Space Administration (NASA) under Contract No. 80KSC021F0014, through Subcontract No. UFL-S-0520 (Task Order 01) with Aegis Aerospace, Inc.

Author Contributions

NJHA conceived the study, established the operational-era framework and the accounting assumptions, contributed to the carbon accounting, developed the Bio-Process Sizing Framework, and supervised the project. JDE led the carbon accounting and its visualization, reconciled all mass and carbon balances, shaped the design of the remaining figures, and composed the Supplementary Information. AK compiled the itemized consumable and hygiene supply tables underlying the carbon accounting. RGI contributed to the figure design and code and parameterized disposition of cellulosics. AYG performed

the initial carbon accounting for wet organic waste, contributed to figure design, and drafted sections of the manuscript. JB performed carbon accounting and bioprocess calculations and produced figures. SD compiled bioprocess parameters from the literature. CHP contributed to the carbon accounting. KHR provided operational input on ISS cargo handling and container re-use, and reviewed the manuscript. AJB contributed to conceptualization, formal analysis, and visualization. All authors wrote, edited, and reviewed the manuscript, and have read and approved the final version.

Competing Interests

The authors declare that they have no conflicts of interest.

References

1. Craig, D. A., Troutman, P. & Herrmann, N. Pioneering Space Through the Evolvable Mars Campaign. In *AIAA SPACE 2015 Conference and Exposition*, DOI: 10.2514/6.2015-4409 (American Institute of Aeronautics and Astronautics, Pasadena, California, 2015).

2. Pitts, R. *et al.* Development of a Predictive Model for In-Situ Resource Utilization of Space Exploration Waste. In *ASCEND 2023*, DOI: 10.2514/6.2023-4659 (American Institute of Aeronautics and Astronautics, Las Vegas, Nevada, 2023).

3. Menezes, A. A., Cumbers, J., Hogan, J. A. & Arkin, A. P. Towards synthetic biological approaches to resource utilization on space missions. *J. The Royal Soc. Interface* **12**, 20140715, DOI: 10.1098/rsif.2014.0715 (2015).

4. Lynch, C. S. *et al.* A Historical Review of Logistics Mass and Crew Time Demands for ISS Operations. In *53rd International Conference on Environmental Systems*, ICES-2024-132 (Louisville, KY, 2024).

5. Leach, H. & Ewert, M. Analysis of Historical International Space Station Logistical Mass Delivery. In *2021 IEEE Aerospace Conference (50100)*, 1–9, DOI: 10.1109/AERO50100.2021.9438212 (IEEE, Big Sky, MT, USA, 2021).

6. Perchonok, M. & Bourland, C. NASA food systems. *Nutrition* **18**, 913–920, DOI: 10.1016/S0899-9007(02)00910-3 (2002).

7. Linne, D. L. *et al.* Waste Management Options for Long-Duration Space Missions: When to Reject, Reuse, or Recycle. In *7th Symposium on Space Resource Utilization*, DOI: 10.2514/6.2014-0497 (American Institute of Aeronautics and Astronautics, National Harbor, Maryland, 2014).

8. Carter, D. L., Tobias, B. & Orozco, N. Y. Status of ISS Water Management and Recovery. In *43rd International Conference on Environmental Systems*, DOI: 10.2514/6.2013-3509 (American Institute of Aeronautics and Astronautics, Vail, CO, 2013).

9. Williamson, J., Wilson, J. P. & Luong, H. Status of ISS water management and recovery. In *53rd International Conference on Environmental Systems*, ICES-2024-317 (Louisville, KY, 2024).

10. Junaedi, C. *et al.* Compact and Lightweight Sabatier Reactor for Carbon Dioxide Reduction. In *41st International Conference on Environmental Systems*, DOI: 10.2514/6.2011-5033 (American Institute of Aeronautics and Astronautics, Portland, Oregon, 2011).

11. Barta, D. SpaceCraft Oxygen Recovery (SCOR) (2026).

12. Sepka, S., Shapiro, A., Ewert, M. & Lee, J. Considerations For Waste-to-Base Future Research Paths. In *2023 International Conference on Environmental Systems* (Calgary, Canada, 2023).

13. Undri, A., Rosi, L., Frediani, M. & Frediani, P. Efficient disposal of waste polyolefins through microwave assisted pyrolysis. *Fuel* **116**, 662–671, DOI: 10.1016/j.fuel.2013.08.037 (2014).

14. Russell, A. D., Antreou, E. I., Lam, S. S., Ludlow-Palafox, C. & Chase, H. A. Microwave-assisted pyrolysis of HDPE using an activated carbon bed. *RSC Adv.* **2**, 6756, DOI: 10.1039/c2ra20859h (2012).

15. Zhang, M. *et al.* Pyrolysis of Polyolefins Using Rotating Arc Plasma Technology for Production of Acetylene. *Energies* **10**, 513, DOI: 10.3390/en10040513 (2017).

16. Jones, H. W. Much lower launch costs make resupply cheaper than recycling for space life support. In *47th International Conference on Environmental Systems*, ARC-E-DAA-TN43292 (Charleston, SC, 2017).

17. Jones, H. W. Take Material to Space or Make It There? In *ASCEND 2023*, DOI: 10.2514/6.2023-4618 (American Institute of Aeronautics and Astronautics, Las Vegas, Nevada, 2023).

18. Kim, M. J. Counting stars and costs: An empirical examination of space launch cost trend at NASA. *Acta Astronaut.* **232**, 633–639, DOI: 10.1016/j.actaastro.2025.04.011 (2025).

19. Barta, D. & Henninger, D. Regenerative life support systems—Why do we need them? *Adv. Space Res.* **14**, 403–410, DOI: 10.1016/0273-1177(94)90329-8 (1994).

20. Strayer, R. F. & Atkinson, C. F. An Overview: Recycling Nutrients from Crop Residues For Space Applications. *Compost. Sci. & Util.* **5**, 25–31, DOI: 10.1080/1065657X.1997.10701882 (1997).

21. Bubenheim, D. L., Flynn, M. T., Lamparter, R., Bates, M. & Kliss, M. Integration of Biological, Physical/Chemical and Energy Efficient Systems in the CELSS Antarctic Analog: Performance of Prototype Systems and Issues for Life Support (Nagoya, Japan, 1998).

22. Wheeler, R. M. Challenges for Life Support Systems in Space Environments, Including Food Production (New Orleans, LA, 2012).

23. Caraccio, A., Poulet, L., Hintze, P. & Miles, J. D. Investigation of bio-regenerative life support and trash-to-gas experiment on a 4 month Mars simulation mission (2014).

24. Straight, C. L., Bubenheim, D. L., Bates, M. E. & Flynn, M. T. The CELSS Antarctic Analog Project: an advanced life support testbed at the Amundsen-Scott South Pole Station, Antarctica. *Life Support. & Biosphere Sci. Int. J. Earth Space* **1**, 52–60 (1994).

25. Cilliers, J., Hadler, K. & Rasera, J. Toward the utilisation of resources in space: knowledge gaps, open questions, and priorities. *npj Microgravity* **9**, 22, DOI: 10.1038/s41526-023-00274-3 (2023).

26. Kruyer, N. S., Realff, M. J., Sun, W., Genzale, C. L. & Peralta-Yahya, P. Designing the bioproduction of Martian rocket propellant via a biotechnology-enabled in situ resource utilization strategy. *Nat. Commun.* **12**, 6166, DOI: 10.1038/s41467-021-26393-7 (2021).

27. Berliner, A. J. *et al.* Space bioprocess engineering on the horizon. *Commun. Eng.* **1**, 13, DOI: 10.1038/s44172-022-00012-9 (2022).

28. Averesch, N. J. H. *et al.* Microbial biomanufacturing for space-exploration—what to take and when to make. *Nat. Commun.* **14**, 2311, DOI: 10.1038/s41467-023-37910-1 (2023).

29. Soundararajan, M. *et al.* Theoretical design of a space bioprocessing system to produce recombinant proteins. *npj Microgravity* **9**, 78, DOI: 10.1038/s41526-023-00324-w (2023).

30. Cui, N. & Pozzobon, V. Food-Grade Cultivation of Saccharomyces cerevisiae from Potato Waste. *AgriEngineering* **4**, 951–968, DOI: 10.3390/agriengineering4040061 (2022).

31. Cai, D. *et al.* Enhanced Bacitracin Production by Systematically Engineering S-Adenosylmethionine Supply Modules in Bacillus licheniformis. *Front. Bioeng. Biotechnol.* **8**, 305, DOI: 10.3389/fbioe.2020.00305 (2020).

32. Wang, Y., Liu, L., Jin, Z. & Zhang, D. Microbial Cell Factories for Green Production of Vitamins. *Front. Bioeng. Biotechnol.* **9**, 661562, DOI: 10.3389/fbioe.2021.661562 (2021).

33. Collier, T. R. V. *et al.* Microbial lipids for a sustainable future: the growing potential of synthetic microbial engineering for consumer oils. *Critical Rev. Biotechnol.* **46**, 477–500, DOI: 10.1080/07388551.2026.2615047 (2026).

34. Jang, Y.-S. *et al.* Engineering of microorganisms for the production of biofuels and perspectives based on systems metabolic engineering approaches. *Biotechnol. Adv.* **30**, 989–1000, DOI: 10.1016/j.biotechadv.2011.08.015 (2012).

35. Koh, S. *et al.* Microbial Platform for Tailor-made Production of a Biodegradable Polylactide Modifier: Ultrahigh-Molecular-Weight Lactate-Based Polyester LAHB. *ACS Sustain. Chem. & Eng.* **12**, 6145–6156, DOI: 10.1021/acssuschemeng.3c07662 (2024).

36. Ewert, M. K. & Stromgren, C. Astronaut mass balance for long duration missions. In *49th International Conference on Environmental Systems*, ICES-2019-126 (Boston, MA, 2019).

37. Lynch, C. S., Goodliff, K. E., Stromgren, C., Vega, J. & Ewert, M. K. Logistics Rates and Assumptions for Future Human Spaceflight Missions Beyond LEO. In *ASCEND 2023*, DOI: 10.2514/6.2023-4617 (American Institute of Aeronautics and Astronautics, 2023).

Supplementary Files

This is a list of supplementary files associated with this preprint. Click to download.

- SI.pdf
- SD.xlsx